

# Characterizing the Spatial Variability of Broadband Albedo in a Semidesert Environment for MODIS Validation

M. J. Barnsley,<sup>\*</sup> P. D. Hobson,<sup>\*</sup> A. H. Hyman,<sup>†</sup> W. Lucht,<sup>†</sup>  
J-P. Muller,<sup>†</sup> and A. H. Strahler<sup>†</sup>

**G**lobal data sets on land surface albedo will be one of the core products to be derived from data acquired by the Moderate Resolution Imaging Spectroradiometer (MODIS), part of NASA's Earth Observing System. Widespread acceptance of this product by the user communities is dependent, in part, on a comprehensive and rigorous programme of calibration and validation. Since the MODIS albedo product will be produced at a spatial resolution of 1 km, while measurements obtained from field instruments typically relate to areas of only a few tens of meters, this requires an understanding of the spatial variability of land surface albedo and a robust means of scaling up from field to satellite measurements. In this article, we examine these issues for a semidesert environment (the PROVE'97 field site at Jornada, New Mexico, USA). Spatial variations in field measurements of broadband albedo are related to the fractional ground cover of different scene elements (live and senescent vegetation, soil and shadow) via a simple linear mixture model. Information on the fractional ground cover of the scene elements is derived from ground-based hemispherical photography. It is shown that the albedo values predicted by the mixture model are accurate to within 2% of the corresponding measured values. This approach offers considerable potential for the validation of MODIS-derived albedo values through the use of spec-

tral mixture modelling applied to fine spatial resolution satellite sensor images. ©Elsevier Science Inc., 2000

## INTRODUCTION

"Terra," the first platform of NASA's Earth Observing System (EOS), is scheduled for launch towards the end of 1999. A number of sensors will be carried on board this satellite, including the Moderate Resolution Imaging Spectroradiometer (MODIS). The MODIS Land (MODLAND) Science Team will produce a suite of scientific products from the data that this sensor gathers, including global data sets on land surface reflectance, temperature and albedo, leaf area index (LAI), the fraction of absorbed photosynthetically-active radiation (*f*APAR), net primary production (NPP), land cover, and land cover change (Justice et al., 1998). A comprehensive and rigorous programme of calibration and validation (Cal/Val) is planned for the postlaunch era to ensure the widespread adoption of these products by the relevant user communities (Privette et al., 1997). Among other things, this will require a comparison against near-simultaneous *in situ* measurements of the same properties obtained using ground-based instruments. Since most of the MODLAND data products will be produced at a spatial resolution of 1 km, while the measurements made by field instruments typically relate to an area of no more than a few tens of meters, this demands an understanding of the spatial variability of the various land surface properties and a robust mechanism for scaling up from field to satellite measurements. The latter may, in turn, involve the use of image data recorded at intermediate spatial scales by other sensors mounted on board aircraft and Earth-orbiting satellites.

<sup>\*</sup> Department of Geography, University of Wales Swansea, Singleton Park, Swansea, United Kingdom

<sup>†</sup> Center for Remote Sensing, Boston University, Boston

<sup>‡</sup> Department of Geomatic Engineering, Gower Street, London, United Kingdom

Address correspondence to M. J. Barnsley, Dept. of Geography, Univ. of Wales Swansea, Singleton Park, Swansea, SA2 8PP, UK. E-mail: M.Barnsley@swansea.ac.uk

Received 31 January 1999; revised 23 December 1999.

A number of calibration/validation sites has been identified at which the *in situ* measurements required to validate MODIS data products are currently being obtained. Some of these have been designated as “core” sites, while others relate to specific data products (Privette et al., 1997). Primary validation is based on the so-called Tier 3 and Tier 4 sites, as defined in the Global Hierarchical Observation system (GHOST) developed by the Global Climate Observing Systems’ Terrestrial Observations Panel for Climate (GCOS-TOPC). These are equipped with a suite of instruments mounted above the observed surface on a fixed tower and provide continuous measurements of a variety of radiometric fluxes and other variables.

To date, MODLAND has coordinated a number of prelaunch field campaigns at the test sites, known as Prototype Validation Exercises (PROVE). Among other things, these are intended to evaluate and refine the instrumentation and measurement sampling strategies that will be used postlaunch. One of these campaigns (PROVE’97) took place in 1997 at the USDA experimental range in Jornada, New Mexico, an area of semidesert vegetation. Data from this campaign are used here to demonstrate how the MODIS albedo data product will be validated. More specifically, the spatial variation in albedo measured *in situ* using ground-based, broadband radiometers is examined. To understand the factors controlling this spatial variation, the relative proportions of different scene elements (i.e., live and senescent leaves, woody material and soil) are estimated from digitized, nadir-viewing, hemispherical photographs of the same sample locations. Models are formulated from these data, relating total and NIR broadband albedo to the relative proportions of the scene elements at a series of sites sampled along five transects. Since estimates of the relative proportions of the same scene elements can be determined over much larger areas by applying spectral mixture modelling to high spatial resolution satellite sensor images (e.g., Landsat-TM/ETM+), this provides a relatively simple means by which point measurements of albedo can be scaled spatially to validate estimates of the same property produced from MODIS data. The study, however, highlights a number of environmental factors which, unless accounted for, may introduce significant bias or error into this process. These include the need to standardize the ground data to a common solar zenith angle and to take into account variations in soil moisture between the sample sites. Appropriate corrections for these factors are determined and applied.

## DETERMINING LAND-SURFACE ALBEDO

Albedo is a parameter of critical importance in understanding both climate and vegetation dynamics. It controls the partitioning of solar radiation at the land surface and the radiative coupling between the land and the at-

mosphere. Spectral albedo  $a_\lambda$  is defined in Eq. (1) as the dimensionless ratio of the solar radiation in a narrow spectral waveband that is reflected in all possible directions from a surface to the solar radiation incident on that surface:

$$a_\lambda \approx \frac{1}{\pi} \int_0^{2\pi} \int_0^1 \rho_\lambda(\theta, \varphi, \theta', \varphi') \mu d\mu d\theta, \quad (1)$$

where  $\rho_\lambda$  is the spectral bidirectional reflectance factor,  $\theta$  and  $\varphi$  are the zenith and azimuth angles of the exitant radiation,  $\theta'$  and  $\varphi'$  are the zenith and azimuth angles of the incident radiation, and  $\mu = \cos \theta$  (Henderson-Sellers and Wilson, 1983; Lewis and Barnsley, 1994).

Various methods have been employed to estimate the albedo of the land surface at scales ranging from the local to the global. For example, ground-based measurements may be made at specific locations using a combination of upward and downward pointing pyranometers, sometimes referred to as an albedometer. While this approach has the advantage of being able to provide high-quality data at frequent spatial and temporal intervals (Lafleur et al., 1997), it is constrained by the limited spatial extent of the measurements, which are essentially point samples (Ohmura and Gilgen, 1993). This is often problematic because albedo varies spatially in response to changes in, among other things, vegetation type, soil substrate, and topography (Ohmura and Gilgen, 1993; Starks et al., 1991). Therefore, individual point-based measurements may not be representative of the surrounding area, unless the land cover, substrate, etc. in the region are reasonably homogeneous (Starks et al., 1991; Minnis et al., 1997). It is possible, of course, to devise a sampling scheme to account for spatial heterogeneity in the observed landscape. Practical considerations, however, most notably the cost of acquiring sufficient field instrumentation, generally mean that this approach is untenable (Starks et al., 1991).

Where albedo data are required over more extensive areas, an alternative approach must be used. One such approach is to determine the albedo of specific land-cover types and to extrapolate these values spatially by means of a land cover map, typically one generated from a satellite-sensor image (Matthews, 1983; Li and Garand, 1994). The limitations inherent in this approach include a) the impact of errors in the land cover classification, b) the spatial and thematic generalization associated with the classification scheme, c) the need to assign “typical” (mean) values of albedo to each land cover category, and d) the difficulty of taking into account the temporal dynamics and natural spatial variability of the land-cover classes employed.

Another approach is to derive estimates of land surface albedo directly from the satellite sensor data. In this context, conventional nadir-viewing images generally provide relatively poor estimates of the surface albedo, owing to the anisotropic scattering of incident solar radia-



Figure 1. Location of Jornada Experimental Range study site (marked by JRN). Source: <http://jornada.nmsu.edu>

tion by most Earth surface materials (Kimes and Sellers, 1985; Kimes et al., 1987). More accurate estimates can be obtained by inverting mathematical models of surface-radiation scattering—known as bidirectional reflectance distribution function (BRDF) models—against image data recorded at several different solar illumination and/or sensor view angles with respect to a given area on the Earth surface (Li and Garand, 1994; Barnsley et al., 1997; Lewis et al., 1998; Wanner et al., 1997). This approach will be used to generate global data sets on albedo from data recorded by the MODIS sensor (Li and Garand, 1994; Lewis et al., 1998; Wanner et al., 1997).

Even so, the requirement for ground-based measurements of albedo remains, most importantly to evaluate the error/accuracy associated with the outputs from the BRDF models applied to the satellite sensor data. In this context, previous studies suggest that a number of environmental factors must be taken into consideration when devising a ground-based validation strategy. These include spatial variations in the target properties (e.g., percentage vegetation cover) (Idso et al., 1975; Allen et al., 1994; DeAbreu et al., 1994), and changes in the solar zenith angle (Lafleur et al., 1997; Allen et al., 1994; Schaaf et al., 1994) and soil moisture content (Minnis et al., 1997; Idso et al., 1975; Allen et al., 1994; Wallace et al., 1990) during the field measurement program.

## STUDY SITE

PROVE'97 took place between 20 and 30 May 1997 at the USDA-ARS/LTER Jornada Experimental Range, 23 miles north of Las Cruces, New Mexico (32.5°N, 106.8°W; Fig. 1). The range consists of a flat valley, approximately 800

km<sup>2</sup> in size, bounded to the east and west by mountains. The main land cover types at this site can be categorized as follows: i) grassland, ii) shrubland, and iii) transitional areas (i.e., mixed grass and shrubs). Only the first and third of these are considered in this study.

The shrubs growing on the sandy soils in the vicinity of the tower at the transitional site are honey mesquite (*Prosopis glandulosa*) and soap tree yucca (*Yucca elata*), while the dominant grass is black grama (*Bouteloua eriopoda*) (Dick-Peddie, 1993). The main land cover categories reflect the slow change from grasses to shrubs that has been taking place following overgrazing of the site at the beginning of the century. The climate is semiarid (280 mm mean annual precipitation between 1961 and 1990) and, as a result, the vegetation cover throughout the valley is sparse, with an average leaf area index (LAI) of 0.5. The occurrence of just a few unpaved roads, data towers, water wells, and fences is such that man-made structures provide a minimal contribution to the scene, particularly in the context of remote sensing data acquired at the spatial resolution associated with MODIS (Kannenburg, 1997).

## DATA SOURCES AND METHODOLOGY

### Albedometers

Surface albedo was measured using a pair of Kipp and Zonen CM14 albedometers (Kipp and Zonen, 1997)—one recording data over the range 305–2800 nm, hereafter referred to as total shortwave broadband albedo, the other operating in the range 695–2800 nm, hereafter referred to as NIR broadband albedo. Broadband albedo at visible wavelengths (i.e., 305–695 nm) can be calculated from these data using information on the visible, NIR, and total irradiance derived from atmospheric radiative-transfer code, such as 6S (Vermote et al., 1997), and contemporaneous measurements of atmospheric optical depth. Both albedometers were mounted on a black tripod at a height of 4.1 m above the surface. The instruments were leveled before taking each set of measurements. A data logger was used to record at least five sets of measurements at each sample location.

The surface albedo was sampled in this way at intervals of 10 m along four short (100 m) transects radiating north, south, east, and west from the main instrumentation tower—the focal point for measurements at the transitional site. Several of these transects were sampled on more than one occasion, under a range of solar illumination conditions. Further measurements were made along a single 1 km transect to the east of the tower. At the grassland site, albedo measurements were taken along a single 150 m transect, sampled at 10 m intervals, at three different times of day (i.e., at different solar zenith angles).

Researchers from the Jet Propulsion Laboratory (JPL) also acquired albedo measurements at the tower site us-

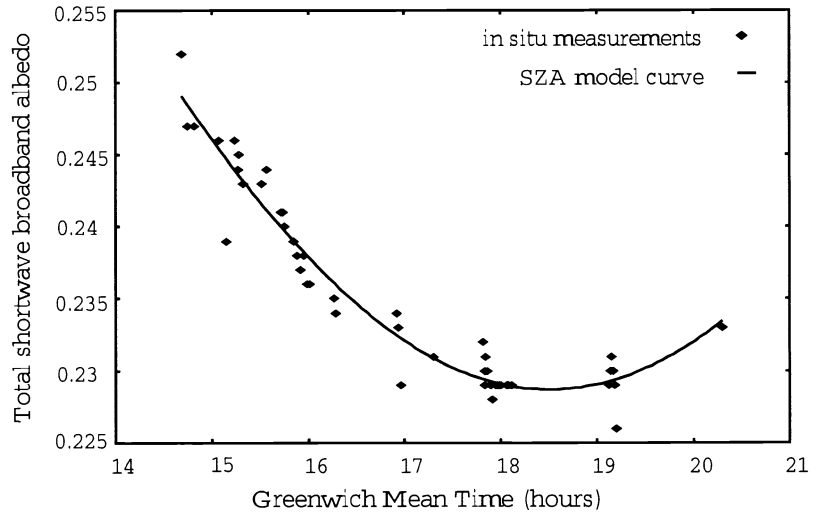


Figure 2. Solar zenith angle correction model derived by fitting a curve to a semidiurnal time-series acquired by the JPL team using their total shortwave broadband Kipp and Zonen CM14 albedometer for a fixed location at the transitional site on 24 May 1997. Local time at Jornada (MDT) was 6 h behind GMT. The form of the model is:  $0.2753 + (0.0466 \sin(0.2546 \text{ GMT}))$ , where GMT is decimalized Greenwich Mean Time.

ing a single, total-shortwave Kipp and Zonen CM14 albedometer. Their measurements include a series readings taken at different times during the day. This information has been used to derive a model to correct our albedo measurements for solar zenith angle effects. The relationship between albedo and solar zenith angle derived from the JPL measurements is similar to that reported in other studies (Lafleur et al., 1997; Idso et al., 1975; Allen et al., 1994; Schaaf et al., 1994), and has the form

$$0.2753 + (0.046 \sin(0.2546 \text{ GMT})), \quad (2)$$

where GMT is decimalized Greenwich Mean Time (Fig. 2). This model was used to normalize the albedo measurements for all other sample locations to their equivalent values at 12 noon MDT (18:00 GMT).

### Hemispherical Photography

In addition to the albedo data, hemispherical photographs were taken at each of the sample sites to provide a visual record of the ground cover observed by the albedometers. The photographs were obtained using a Minolta X-300 SLR camera equipped with a  $150^\circ$  field-of-view “fish-eye” lens. The camera was mounted on the same tripod and at the same height above the ground as the albedometers. This provided standard color images covering  $>90\%$  of the area contributing to the signal recorded by the albedometers. Given that the albedometers and camera could not be mounted on the tripod simultaneously, the photography was acquired immediately after the albedo measurements. The photographs were processed directly into Kodak PhotoCD™ format which provides digital images at a much higher spatial resolution and geometric fidelity that can be achieved using a standard flatbed or film scanner.

A supervised image classification algorithm was used to convert the resultant 24-bit, three-channel images into hemispherical maps of the following scene elements: i) bare soil, ii) gray vegetation (primarily dormant grass),

iii) woody material, and iv) live green vegetation. For each image, a binary mask was defined to exclude the tripod and operators from further analysis. In view of systematic brightness variations within each image, as a result of bidirectional reflectance effects, a principal component transformation was applied to the hemispherical photographs prior to image classification. The angle-dependent brightness variations were found to be concentrated in the third principal component; consequently, this channel was excluded from the classification process. Examples of the original and classified hemispherical photographs for two sites exhibiting, respectively, high and low levels of green biomass are presented in Figures 3a and 3c. Given the nature of the images, it was not possible to perform a traditional accuracy assessment of the resultant classifications. Nevertheless, a qualitative, visual inspection suggests that a high level of accuracy has been achieved.

To calculate the proportion of each scene element in the hemispherical photographs and, hence, to assess their influence on the albedometer measurements, corrections were made for the effect of camera lens distortion and the spatial response function of the albedometers. These data were then used, in conjunction with the corresponding albedo measurements, to derive a simple linear mixture model for each sample site:

$$a = \beta_1 P_{\text{soil}} + \beta_2 P_{\text{grey veg}} + \beta_3 P_{\text{woody veg}} + \beta_4 P_{\text{live veg}} + \varepsilon, \quad (3)$$

where  $a$  is the measured albedo and  $P_\lambda$  is the  $\sin^{-1} \sqrt{p}$  transformed weighted proportion,  $p$ , of scene element  $x$ , and  $\varepsilon$  is an error term. Values of the coefficients  $\beta_1$ ,  $\beta_2$ ,  $\beta_3$ , and  $\beta_4$  were derived using least-squares estimation.

## RESULTS

### Day-to-Day Stability in the Albedo Data

Figure 4 shows plots of total shortwave and NIR broadband albedo along the north transect at the transitional

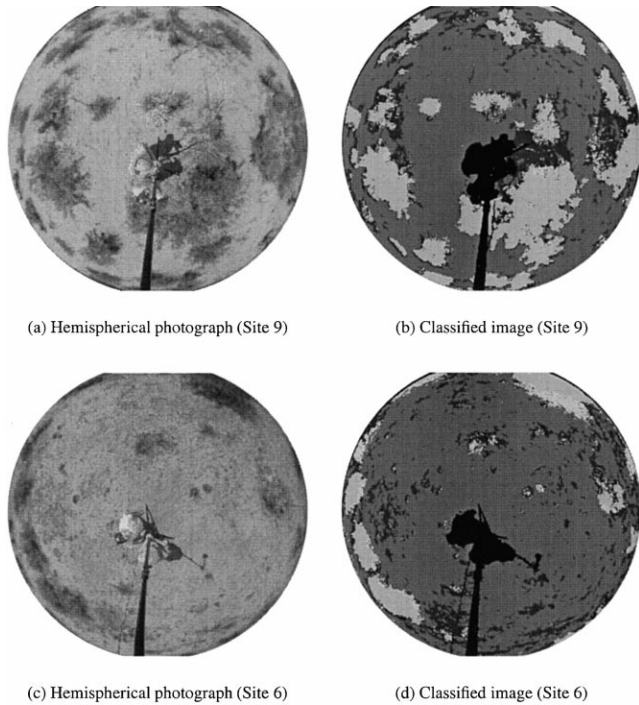


**Figure 3.** Hemispherical photographs and classified images of site 9 (high green biomass) and site 6 (low green biomass) on the north transect. Classification key: red=soil, green=live vegetation, blue=grey vegetation, cyan=dead/bare woody vegetation.

site. These data were acquired at approximately the same time of day on 22, 23, and 26 May and have been adjusted to the equivalent values at solar noon (MDT) using the solar zenith angle correction model [Eq. (2)]. The most important feature of this diagram is that the variations in albedo along the transect appear to be replicated fairly consistently from day to day, albeit that they differ in terms of absolute value. This gives us confidence that the observed patterns are a response to real variations in surface properties (notably changes in vegetation cover). For example, the lower albedo values at sites 4–6 are associated with higher proportions of vegetation cover (Fig. 3a), while the higher albedo values at sites 7–9 are associated with sites dominated by bare soil (Fig. 3c). Despite the small range in albedo values, the similar trends along the transect for all three days suggests that the controlling factor is the proportion of different scene elements falling within the albedometers' field-of-view, rather than random fluctuations or errors in the measurements.

### Diurnal Variations in Albedo

The three data sets reported in Figure 4 were acquired at roughly the same local solar time on different days, such that the effect of variations in the solar zenith angle between data acquisitions is believed to be minimal. Figure 5a, on the other hand, demonstrates the influence

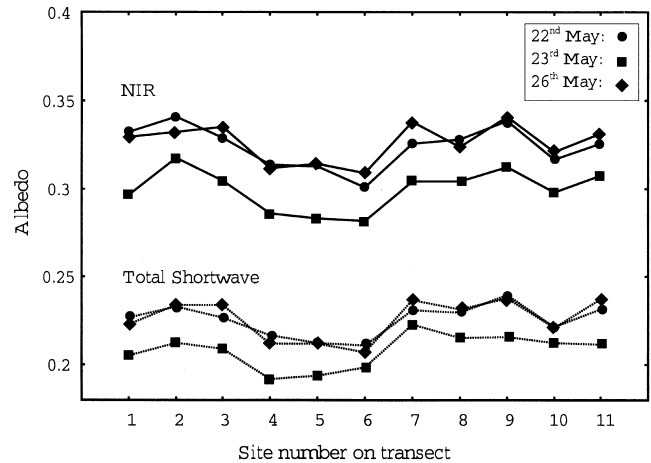


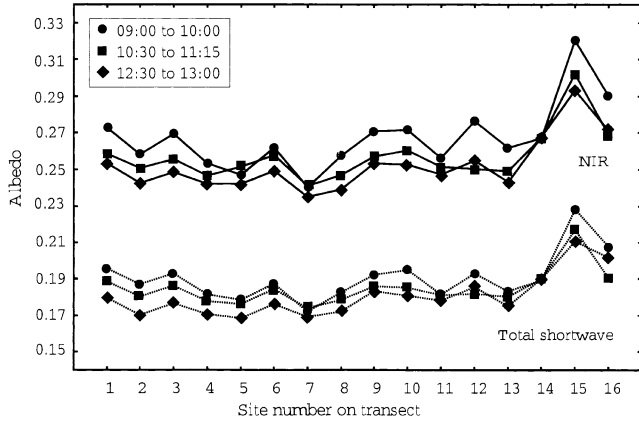
**Figure 4.** Total shortwave and NIR broadband albedo measurements (corrected for solar zenith angle) along the grassland transect for 22, 23, and 26 May 1997.

of solar zenith angle effects on data collected along the grassland site transect. Using data recorded at three different times of day (09:00–10:00, 10:30–11:15, and 12:30–13:00) on 27 May, it shows that the albedo value recorded at each site decreases progressively from early morning to midday in both the total shortwave and NIR wavebands. More importantly, the variation in albedo as a function of changing solar zenith angle is approximately the same magnitude as the variation between sample sites (i.e., along the transect), if site 15 is excluded. This suggests that it is essential to correct for the effects of solar zenith angle if spatial variations in albedo are to be interpreted correctly.

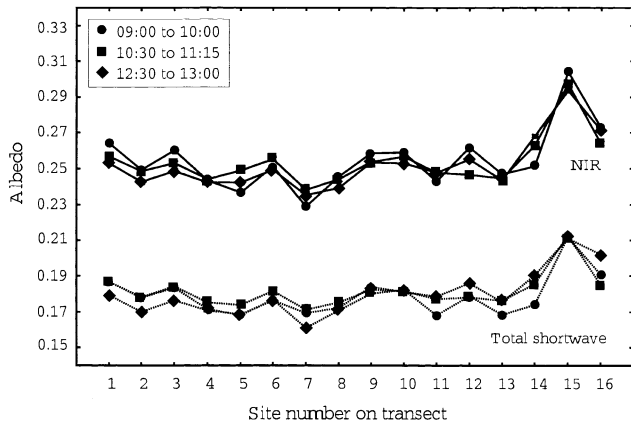
Figure 5b shows the total shortwave and NIR broadband albedo measurements for the grassland transect after correction for solar zenith angle effects. The close correspondence between the data acquired at each of the three times of day is now evident. The residual variation between the different measurements of the same sample locations is probably due to slight differences in the positioning of the albedometers, although every effort was made to minimize this. It is also possible, though less likely, that the residual variations are due to subtle changes in the vegetation canopy, even over this short sampling period (i.e., 09:00–13:00). Finally, it should be noted that the solar zenith angle correction model [Eq. (2)] was formulated from measurements made at a site with a mixture of soil, grass and other vegetation typical of the transitional land-cover category, whereas the data in Figure 5 pertain to the grassland transect for which, not surprisingly, the proportion of dormant grass is considerably higher.

### Other Environmental Effects

Despite correcting the albedo data for solar zenith angle effects, initial attempts to model quantitatively the rela-



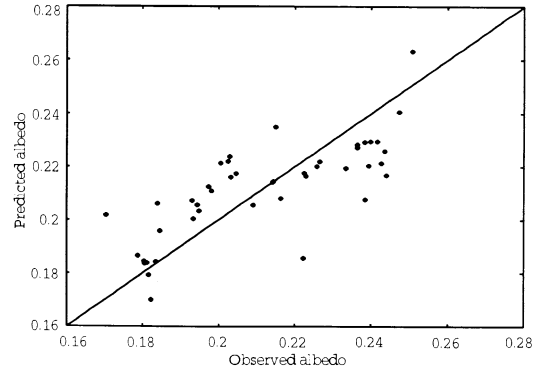
(a)



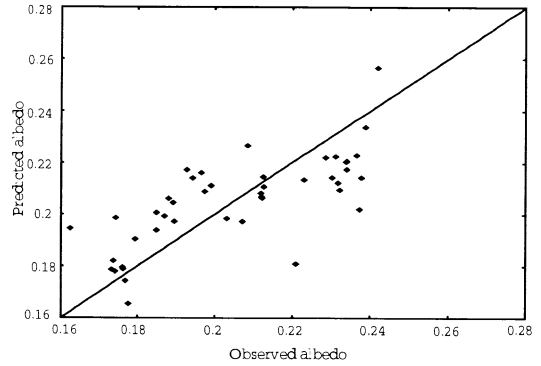
(b)

Figure 5. Total shortwave and NIR broadband albedo measurements along the grassland transect for three times on the 27 May 1997: (a) without solar zenith angle correction and (b) corrected for solar zenith angle.

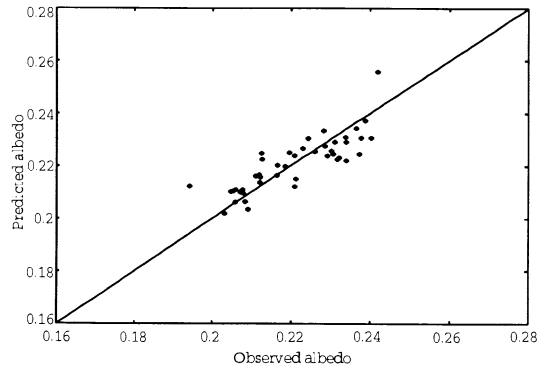
relationship between broadband albedo and the relative proportions of different scene elements using a linear mixture model [Eq. (3)] resulted in relatively poor fits between the observed and modelled albedo values (Figs. 6b and 7b). More specifically, there is evidence of a systematic bias, such that the modeled values appear to overestimate the observations for some, relatively low albedo sites and to underestimate them at other, relatively high albedo sites. The most likely explanation for this seems to be differences in the reflectance of the soil substrate before and after precipitation events. Evidence to support this supposition can be found in Figure 4, which highlights the consistently lower albedo values reported along the north transect on 23 May, compared to the data recorded along the same transect on 22 and 26 May. The difference can be accounted for by a small (1.6 mm) precipitation event which occurred during the late



(a)

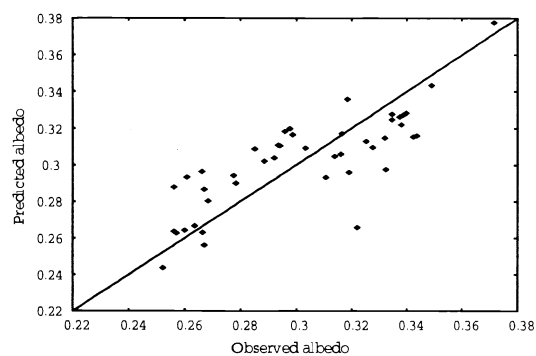


(b)

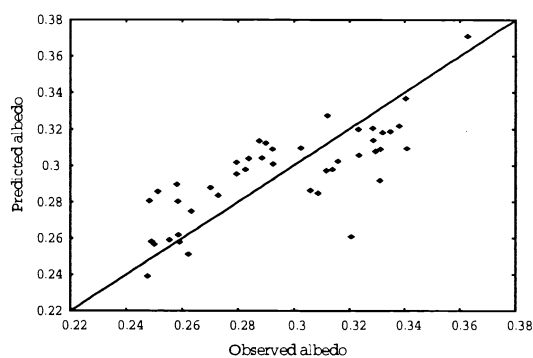


(c)

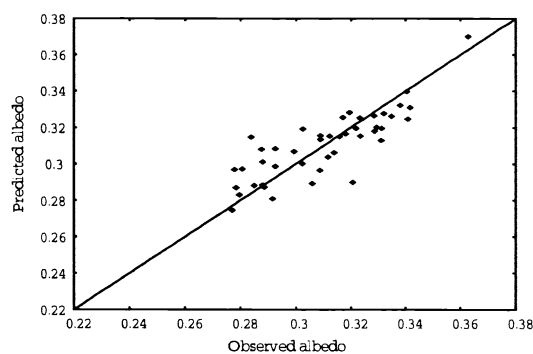
Figure 6. Observed versus predicted values for total shortwave broadband albedo: (a) without corrections to observed values for solar zenith angle or soil moisture effects, (b) with corrections for solar zenith angle but not soil moisture effects and (c) with corrections for both solar zenith angle and soil moisture effects.



(a)



(b)



(c)

Figure 7. Observed versus predicted values for NIR broadband albedo: (a) without corrections to observed values for solar zenith angle or soil moisture effects, (b) with corrections for solar zenith angle but not soil moisture effects and (c) with corrections for both solar zenith angle and soil moisture effects.

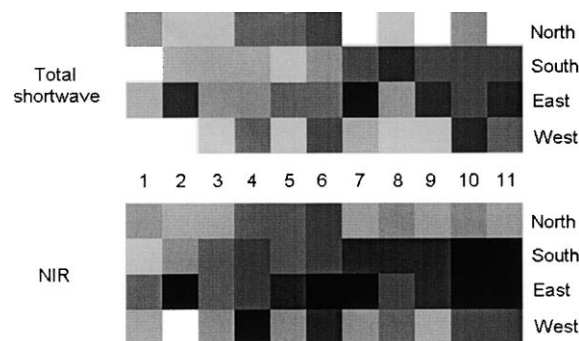


Figure 8. Schematic representation of the total shortwave and NIR albedo values measured along the north, south, east, and west transects having applied corrections for solar zenith angle and soil moisture. The numbers given in the center of the figure are location identifiers, with lower numbers representing sites closer to the tower site. Shortwave broadband albedo values vary from 0.194 (black) to 0.242 (white), while corresponding values for the NIR vary between 0.277 (black) and 0.363 (white). The grayscale values have been linearly stretched between these minimum and maximum values.

afternoon of 22 May (J. Privette, personal communication). Despite the rapid drying of the soil substrate that might be expected to occur due to the effects of wind, solar radiation, and the normal vapor pressure deficit in desert environments, Figure 4 suggests that this rainfall event continued to affect the reflectance of the soil substrate the following morning (i.e., on 23 May). This might be a direct result of an increased soil moisture content or an indirect result of the rainfall due to “pitting” of the soil surface by the raindrops (i.e., due to an increase in shadowing caused by the rougher surface micro-topography). Similar reductions in albedo values were also noted in the data recorded along the south and east transects on 23 May.

A simple scaling factor was calculated to correct the data for the soil moisture/microtopography effects, using albedo measurements obtained at one of the sites on the south transect at the same time of day on 23 May and 26 May (i.e., the day after the rainfall event and several days later, when the surface might be expected to have dried out and the effects of surface pitting erased by wind-blown sand). This scaling factor was applied to all of the data believed to have been affected by the precipitation event.

### Spatial Variations in the Corrected Albedo Values

Figure 8 presents a schematic representation of the albedo values measured along all four transects radiating from the transitional (tower) site after correction for the effects of solar zenith angle and soil moisture. Observed values of total short-wave broadband albedo vary between

Table 1. Regression Model Coefficients Using Percent Albedo Values Corrected for Solar Zenith Angle and Soil Moisture Effects

Variable	Total Shortwave Albedo	NIR Albedo
Soil	17.6671°	25.8978°
Gray (dormant) vegetation	6.8581°	6.1305°
Woody vegetation	0.3108	0.4462
Live vegetation	5.9482°	10.0310°
$R^2$	0.7	0.69
RMSE (Albedo)	±0.014	±0.025

° Denotes significant at the 95% level.

0.194 and 0.242, while those in the NIR vary between 0.277 and 0.363. The grayscale values presented in Figure 8 have been linearly stretched between these minimum and maximum values. The lower albedo values at the far end of the south and east transects. (i.e., sites 7–11) are associated with greater proportions of gray vegetation. The remainder of the sites along these and the other two transects exhibit higher albedo values as a result of their greater proportion of bare soil. Even so, there is clearly considerable variability in the measured albedo in the vicinity of the tower.

### Comparison of Observed and Predicted Albedo Values

Having corrected the measured albedo values for the effects of solar zenith angle and soil moisture, the linear mixture models relating observed albedo to the weighted proportions of the four main scene elements (i.e., soil substrate, live green vegetation, dormant grey vegetation, and woody material) were recalculated. The models formed in this way were found to be highly significant (overall F-test:  $p < 0.001$ ) for both total shortwave and NIR broadband albedo. The model coefficients are given in Table 1. With the exception of the proportion of woody vegetation, all are statistically significant at the 95% level. The limited contribution of the woody material to the model is due to the fact that it constitutes such a small proportion of the total ground cover at most of the sample sites. Nevertheless, we have retained this variable in the linear mixture model since, ultimately, all of the scene elements contribute to the observed albedo.

The resultant  $R^2$  values for the models are 0.7 for the total shortwave and 0.69 for the NIR; in other words, knowledge of the relative proportions of ground covered by exposed soil, gray (dormant) vegetation, woody vegetation, and live green vegetation explains 70% and 69% of the observed variation in total shortwave and NIR broadband albedo, respectively. The estimated root mean squared errors (RMSEs) for the two models suggest that the total shortwave albedo may be predicted to within ±0.014 and NIR albedo to ±0.025. A graphical comparison between the observed albedo values (corrected for both solar zenith angle and soil moisture effects) and the

albedo values predicted by the linear mixture model of scene elements is presented in Figures 6c and 7c.

### Testing the Model

The predictive ability of the linear mixture model was tested using an independent set of albedo measurements (i.e., data not used in the model formulation) recorded at the seven sites furthest along the 1 km transect to the east of the tower. Each of these locations has a different mixture of the four main scene elements, varying from soil-dominated sites to ones with a significant amount of vegetation. The relative proportions of these scene elements at each of the seven sites were derived from the classified images and used as input to the linear mixture models, based on the regression coefficients given in Table 1. The resultant values of albedo predicted by the models are reported in Table 2, in addition to the observed (corrected) albedo values for the same sites. This information is also presented graphically in Figure 9.

The mean difference between the observed (corrected) and predicted values across all seven sites in 0.0047 for the total shortwave broadband albedo and 0.0057 for the NIR broadband albedo, respectively. These differences are statistically insignificant at the 95% confidence level (Table 2). They also represent less than 2% of the observed (corrected) albedo value in both bands, which is better than the accuracy of the pyranometers (ca.3%) for an instantaneous measurement. On a site-by-site basis, the largest errors are obtained for locations with the highest proportions of exposed soil. This is probably because the observed albedo values for these sites fall outside the range used to formulate the linear mixture model.

## DISCUSSION

The results presented in the previous section suggest that the linear mixture model derived in this study could be used to estimate accurately the total shortwave and NIR broadband albedo values for locations other than those sampled with the pyranometers. This would require information on the relative proportions of the four main scene elements present in this area, namely soil, live green vegetation, dormant (grey) vegetation, and

Table 2. Observed and Predicted Total Shortwave and NIR Broadband Albedo for the Seven Sample Sites Farthest along the 1 km Transect to the East of the Tower

Site Identifier	Total Shortwave Albedo			NIR Broadband Albedo		
	Observed	Predicted	$\Delta$	Observed	Predicted	$\Delta$
1	0.2385	0.2373	0.0120	0.3366	0.3385	-0.0019
2	0.2350	0.2380	-0.0030	0.3359	0.3398	-0.0039
3	0.2204	0.2202	0.0002	0.3240	0.3144	0.0096
4	0.2538	0.2398	0.0140	0.3558	0.3420	0.0138
5	0.2572	0.2496	0.0076	0.3652	0.3588	0.0064
6	0.2351	0.2350	0.0001	0.3438	0.3355	0.0083
7	0.2293	0.2276	0.0017	0.3322	0.3241	0.0081
$\bar{x}$	0.2385	0.2356	0.0047	0.3419	0.3362	0.0057
$\sigma$	0.0121	0.0086	0.0061	0.0132	0.0130	0.0059

woody material. This information could be obtained by means of spectral unmixing applied to multispectral or hyperspectral image data recorded by airborne or fine spatial resolution satellite sensors. In this way, it should be possible to scale-up from a relatively limited set of ground-based, point samples of albedo to validate the outputs of albedo estimation algorithms applied to global imaging devices, such as MODIS.

One potential problem with this approach, however, is that most fine spatial resolution imaging sensors are nadir-viewing and acquire data within a relatively narrow field-of-view. The estimates of the scene element fractions derived from such data are therefore likely to differ from those generated using the hemispherical (i.e., very wide field-of-view) photography employed in this study. It is difficult to assess the impact of this from the data used in this study, but it clearly deserves detailed consideration prior to “operational” application of the methods developed here.

There is also evidence that the accuracy with which the linear mixture model predicts albedo decreases over very sparsely vegetated sites, owing to the fact that sites

of this nature were not used to parametrize the model. This could be rectified relatively easily by extending the field sampling scheme to incorporate a few extra sites exhibiting very low levels of vegetation cover.

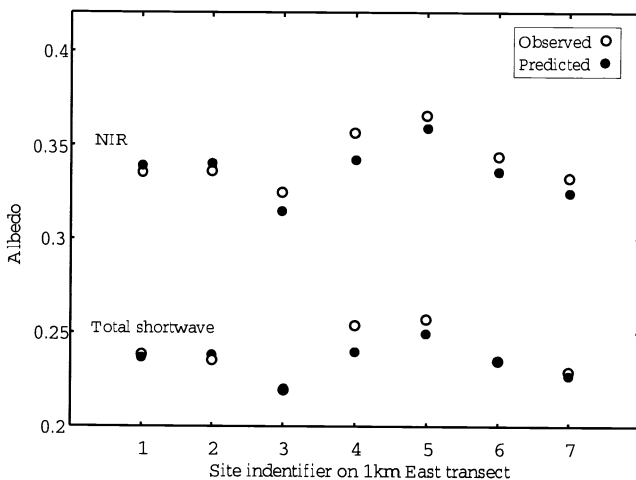
Two other factors also deserve attention. First, some of the measurements made using the albedometers were acquired at spatial intervals of only 10 m along the short (100 m) transects radiating from the tower site. Given the fact that the downward-looking pyranometers record exitant radiation over the entire hemisphere beneath them, it might be thought that such closely spaced samples would exhibit a high degree of spatial autocorrelation (i.e., due to the large degree of overlap between the areas sampled from successive points along the transect). This was tested using a standard measure of spatial autocorrelation, known as Moran’s  $I$  (Wartenberg, 1985), and was found to be insignificant for data from the total shortwave albedometer ( $I=0.096355$ ,  $z=0.756$ ,  $p=0.225$ , where large values of  $I$  indicate greater spatial autocorrelation), but statistically significant in data from the NIR sensors ( $I=0.39949$ ,  $z=2.674$ ,  $p=0.004$ ). The reason for this difference is not clear at present, but overall we do not believe that spatial autocorrelation between sample measurements is a significant problem in this study.

Second, albedo has been predicted using a simple linear mixture model, whereas the relatively high reflectance of the soil substrate at visible wavelengths and of the live, green vegetation at NIR wavelengths is likely to induce a nonlinear relationship with their percentage ground cover due to multiple scattering effects. This might explain why the  $R^2$  values obtained when fitting the linear mixture models to the relative proportions of different scene elements were not higher. On the other hand, the resultant values of albedo predicted by these simple linear models were accurate to within 2% of the observed (corrected) values, so that the significance of this simplification is debatable.

## CONCLUSIONS

This article began by noting that spatial variation in the albedo of the land surface at the local scale complicates

Figure 9. Observed and predicted values of total shortwave and NIR broadband albedo for the seven sample sites furthest along the 1 km transect to the east of the tower.



validation of albedo data sets derived from coarse spatial resolution imaging sensors, such as MODIS on NASA's forthcoming Terra satellite. This is because ground-based measurements typically pertain to areas of only a few tens of meters, whereas MODIS has a spatial resolution of 1 km. In most instances, therefore, where the land cover varies spatially at scales of meters to kilometers, a single ground-based measurement of albedo cannot be used to validate an estimate of the same property derived from the satellite sensor data. Some means of scaling-up from the ground-based measurements to the satellite sensor data is required.

A simple solution to this problem has been developed in this study and applied to data recorded over a semidesert environment, as part of the PROVE'97 field experiment. The method involves the use of a linear mixture model to relate the proportions of the ground covered by each of four primary scene elements [soil, dormant (grey) vegetation, live green vegetation, and woody material] to the broadband albedo of the same area of ground. Information on the former was derived from digitized hemispherical photographs, while the latter was measured using a pair of broadband albedometers. After normalizing the ground-based measurements of albedo to a common solar zenith angle and correcting them for the effects of variations in soil moisture, the observed and predicted values of albedo were shown to differ by less than 2% of the measured value. Since estimates of the proportional ground cover of the same scene elements can be determined over much larger areas by applying spectral mixture modeling to fine spatial resolution satellite sensor images (e.g., Landsat-TM/ETM+), this provides a relatively simple means by which point measurements of albedo can be scaled spatially to validate estimates of the same property produced from MODIS data.

---

*We would like to thank the organizers of PROVE'97, in particular Jeff Privette, for their assistance at various stages in this project. Our thanks also go to Jim Conel and Mark Helmlinger of JPL, for the provision of the additional albedo data. This work was partially funded by the NERC (GR3/11639) in the United Kingdom and NASA (MODIS project, NAS5-31369) in the United States.*

## REFERENCES

- Allen, S., Wallace, J., Gash, J., and Sivakumar, M. (1994), Measurements of albedo variation over natural vegetation in the Sahel. *Int. J. Climatol.* 14:625–636.
- Barnsley, M., Lewis, P., Sutherland, M., and Muller, J. (1997), Estimating land surface albedo in the HAPEX-Sahel southern super-site: inversion of two BRDF models against multiple angle ASAS images. *J. Hydrol.* 189:749–778.
- DeAbreu, R., Keu, J., Maslanik, J., Serreze, M., and LeDrew, E. (1994), Composition of *in situ* and AVHRR-derived broadband albedo over Arctic sea ice. *Arctic* 47:288–297.
- Dick-Peddie, W. (1993), *New Mexico Vegetation, Past, Present and Future*, University of New Mexico Press, Albuquerque, 244 pp.
- Henderson-Sellers, A., and Wilson, M. (1983), Surface albedo data for climate modelling. *Rev. Geophys. Space Phys.* 21: 1743–1778.
- Idso, S., Jackson, R., Reginato, R., Kimball, B., and Nakayama, F. (1975), The dependence of bare soil albedo on soil water content. *J. Appl. Meteorol.* 14:109–113.
- Justice, C., Vermote, E., Townshend, J., et al. (1998), The Moderate Resolution Imaging Spectroradiometer (MODIS): land remote sensing for global change research. *IEEE Trans. Geosci. Remote Sens.* 36:1228–1249.
- Kannenburg, B. (1997), Grassland Prototype Validation Exercise (PROVE) at Jornada Experimental Range. *Earth Obs.* 9:16–18.
- Kimes, D., and Sellers, P. (1985), Inferring hemispherical reflectance of the Earth's surface for global energy budgets from remotely-sensed nadir or directional radiance values. *Remote Sens. Environ.* 18:205
- Kimes, D., Sellers, P., and Diner, D. (1987), Extraction of spectral hemispherical reflectance (albedo) of surfaces from nadir and directional reflectance data. *Int. J. Remote Sens.* 8:1727–1746.
- Kipp and Zonen (1997), *Instruction Manual CM11/CM14 Pyranometer*, Kipp and Zonen, B. V., Delft, Netherlands, 34 pp.
- Lafleur, P., Wurtele, A., and Duguay, C. (1997), Spatial and temporal variations in surface albedo of subarctic landscape using surface-based measurements and remote sensing. *Arctic Alpine Res.* 29:261–26.
- Lewis, P., and Barnsley, M. (1994), Influence of the sky radiance distribution on various formulations of the Earth surface albedo. In *Proceedings of the Sixth International Symposium on Physical Measurements and Signatures in Remote Sensing*, ISPRS, Commission VII, ISPRS, Val d'Isere, France, pp. 707–713.
- Lewis, P., Disney, M., Barnsley, M., and Muller, J.-P. (1998), Deriving albedo for HAPEX-Sahel from ASAS data using kernel-driven BRDF models. *Hydrol. Earth Sys. Sci.*:1–13.
- Li, Z., and Garand, L. (1994), Estimation of surface albedo from space—a parameterization for global application. *J. Geophys. Res. Atmos.* 99:8335–8350.
- Matthews, E. (1983), Global vegetation and land-use: new high resolution databases for climate studies. *J. Climatol. Appl. Meteorol.* 22:474–487.
- Minnis, P., Mayor, S., Smith, W., and Young, D. (1997), Asymmetry in the diurnal variation of surface albedo. *IEEE Trans. Geosci. Remote Sens.* 35:879–891.
- Ohmura, A., and Gilgen, H. (1993), Re-Evaluation of the Global Energy Balance, Interactions between Global Climate Subsystems: the Legacy of Hann, Vol. 75, American Geophysical Union, Washington, DC, pp. 93–110.
- Privette, J., Eck, T., and Deering, D. (1997), Estimating spectral albedo and nadir reflectance through inversion of simple BRDF models with AVHRR/MODIS-like data. *J. Geophys. Res. Atmos.* 102:29,529–29,542.
- Schaaf, C., Li, X., and Strahler, A. (1994), Topographic effects on bidirectional and hemispherical reflectances calculated with a geometric-optical canopy model. *IEEE Trans. Geosci. Remote Sens.* 32:1186–1193.
- Starks, P., Norman, J., Blad, B., Waltershea, E., and Walthall,

- C. (1991), Estimation of shortwave hemispherical reflectance (albedo) from bidirectionally reflected radiance data. *Remote Sens. Environ.* 38:123–134.
- Vermote, E., Tanré, D., Deuze, J., Herman, M., and Morcrette, J. (1997), Second simulation of the satellite signal in the solar spectrum, 6S: an overview. *IEEE Trans. Geosci. Remote Sens.* 35:675–686.
- Wallace, J., Gash, J., and Sivakumar, M. (1990), Preliminary measurements of net radiation and evaporation over baer soil and fallow bushland in the Sahel. *Int. J. Climatol.* 10: 203–210.
- Wanner, W., Strahler, A., Hu, B., et al. (1997), Global retrieval of bidirectional reflectance and albedo over land from EOS MODIS and MISR data: theory and algorithm. *J. Geophys. Res. Atmos.* 102:17,143–17,161.
- Wartenberg, D. (1985), Multivariate spatial correlation: a method for exploratory geographical analysis. *Geogr. Anal.* 17:263–283.